

In Vivo Determination of Bone Structure in Postmenopausal Women: A Comparison of HR-pQCT and High-Field MR Imaging

Galateia J Kazakia,¹ Benedict Hyun,¹ Andrew J Burghardt,¹ Roland Krug,¹ David C Newitt,¹ Anne E de Papp,²
Thomas M Link,¹ and Sharmila Majumdar¹

ABSTRACT: Bone structural measures obtained by two noninvasive imaging tools—3T MRI and HR-pQCT—were compared. Significant but moderate correlations and 2- to 4-fold discrepancies in parameter values were detected, suggesting that differences in acquisition and analysis must be considered when interpreting data from these imaging modalities.

Introduction: High-field MRI and high resolution (HR)-pQCT are currently being used in longitudinal bone structure studies. Substantial differences in acquisition and analysis between these modalities may influence the quantitative data produced and could potentially influence clinical decisions based on their results. Our goal was to compare trabecular and cortical bone structural measures obtained in vivo by 3T MRI and HR-pQCT.

Materials and Methods: Postmenopausal osteopenic women ($n = 52$) were recruited for this study. HR-pQCT imaging of the radius and tibia was performed using the XtremeCT scanner, with a voxel size of $82 \times 82 \times 82 \mu\text{m}^3$. MR imaging was performed on a 3T Signa scanner using SSFP imaging sequences, with a pixel size of $156 \times 156 \mu\text{m}^2$ and slice thickness of $500 \mu\text{m}$. Structure parameters were calculated using standard HR-pQCT and MRI analysis techniques. Relationships between measures derived from HR-pQCT, MRI, and DXA were studied.

Results: Significant correlations between HR-pQCT and MRI parameters were found ($p < 0.0001$) and were strongest for Tb.N ($r^2 = 0.52$), Ct.Th ($r^2 = 0.59$), and site-specific Tb.Sp ($r^2 = 0.54$ – 0.60). MRI and HR-pQCT provided statistically different values of structure parameters ($p < 0.0001$), with BV/TV and Tb.Th exhibiting the largest discrepancies (MR/HR-pQCT = 3–4). Although differences in the Tb.N values were statistically significant, the mean differences were on the order of our reproducibility measurements. Systematic differences between MRI and HR-pQCT analysis procedures leading to discrepancies in cortical thickness values were observed, with MRI values consistently higher. Minimal correlations were found between MRI or HR-pQCT parameters and DXA BMD or T-score, except between HR-pQCT measures at the radius and the ultradistal radius T-scores, where moderate correlations were found ($r^2 = 0.19$ – 0.58).

Conclusions: This study provides unique insight into two emerging noninvasive tools for bone structure evaluation. Our findings highlight the significant influence of analysis technique on results of in vivo assessment and underscore the importance of accounting for these differences when interpreting results from these modalities.

J Bone Miner Res 2008;23:463–474. Published online on November 26, 2007 doi: 10.1359/JBMR.071116

Key words: high-resolution pQCT, MRI, bone structure, image analysis, osteoporosis

INTRODUCTION

OSTEOPOROSIS IS A CONDITION characterized by loss of bone mass and deterioration of microarchitecture and manifests clinically as an increased incidence of fracture.⁽¹⁾ Currently, determination of osteoporotic status is based primarily on BMD values obtained through areal or volumetric X-ray-based imaging techniques. BMD has been shown

to have use in predicting bone strength, and has been proven to be clinically useful in predicting fracture in prospective studies.^(2,3) However BMD does not entirely determine fracture risk^(4,5) or adequately assess the impact of therapeutic interventions.^(6,7) For these reasons, much interest currently exists in the study of other factors associated with bone mechanical competence, including whole bone geometry, cortical and trabecular microstructure, and tissue composition.

Structural analysis is critical in understanding bone mechanics, assessing fracture risk, and evaluating responses to

Anne de Papp is an employee of Merck & Co. All other authors state that they have no conflicts of interest.

¹Musculoskeletal and Quantitative Imaging Research Group, Department of Radiology, University of California, San Francisco, California, USA; ²Merck & Co., West Point, Pennsylvania, USA.

disease, age, and therapy. Improved predictions of biomechanical properties have been found as a result of including measures of bone structure in statistical regressions.^(8–10) Bone structure has been shown to discriminate fracture cases from controls independent of areal BMD.⁽¹¹⁾ Trabecular bone structure is also critical in the evaluation of therapeutic interventions, enabling researchers to explain a greater proportion of the effect of drugs on fracture risk than BMD alone.^(12,13) Therefore, structural analysis is a particularly important aspect of bone quality assessment.

Recent technological advances have made possible non-invasive assessment of bone structure, which is desirable in longitudinal clinical studies. MRI at high-field strength now allows in vivo imaging at resolutions approaching trabecular dimensions. High-resolution (HR)-pQCT imaging is capable of producing isotropic voxels approximately equivalent to trabecular dimensions. Both of these imaging modalities are currently being used in longitudinal clinical studies evaluating osteoporosis therapies. However, these techniques rely on new and advanced technologies and require detailed study and validation before they transition to standard clinical use.

MRI and HR-pQCT differ in many important ways in both acquisition and analysis. These substantial differences may influence the quantitative data produced by these imaging techniques, and therefore could in the future influence clinical or therapeutic decisions based on their results. In *ex vivo* experiments, trabecular and cortical structure measures calculated from both MRI and HR-pQCT have been shown to be highly correlated to those obtained by μ CT imaging, the current gold standard for 3D structural analysis.^(14,15) No equivalent gold standard exists for the in vivo imaging environment. However, comparing measures obtained from these two modalities to each other and to areal BMD may be instructive in understanding how they perform in the in vivo scenario.

In this context, our goal was to compare trabecular and cortical bone structural measures obtained in vivo by 3T MRI and HR-pQCT. We performed this comparison in a cohort of early postmenopausal women with osteopenia as determined by areal BMD. Our specific objectives were to (1) compare trabecular bone structure measures obtained by MRI and HR-pQCT in the distal radius and tibia; (2) compare cortical thickness measurements as calculated by MRI and HR-pQCT in the distal radius and tibia; (3) correlate measures obtained by both modalities with areal BMD measures at the distal radius, proximal femur, and lumbar spine; and (4) investigate variations in bone structure along the length of the imaged regions to determine the need for consistent spatial alignment in cross-modality comparisons. Through comparative analysis using a large cohort, this study provides unique insight into two cutting-edge noninvasive tools for bone structure assessment.

MATERIALS AND METHODS

Subjects

Community-dwelling ambulatory postmenopausal women defined as osteopenic by WHO criteria⁽¹⁶⁾ were

recruited for a longitudinal pilot study comparing the effects of alendronate to placebo on bone microarchitecture. The women were included if they were between the ages of 45 and 65 yr and had been postmenopausal for at least 1 but not more than 6 yr. They were required to exhibit low BMD (T-score range -1.1 to -2.5) by DXA either at the lumbar spine or at the total proximal femur, trochanter, or neck regions of interest. History of or evidence for metabolic bone disease other than postmenopausal bone loss was an exclusion criterion, as was treatment within the previous year with any compound known to influence bone turnover. All imaging described herein occurred at the baseline visit (recruitment completed February 2007).

Fifty-three postmenopausal women were initially enrolled in the study. One subject was excluded from analysis because of incorrect reference line placement in the tibial HR-pQCT scan. Therefore, the complete sample size was 52 women. Of these subjects, four could not tolerate the prone position required for the MRI wrist scan. These subjects were excluded in analyses of radius measures. The study protocol was approved by the UCSF Committee of Human Research, and all patients gave written informed consent before participation.

DXA measurements

Bone densitometry data were acquired using DXA and used to calculate T-scores. DXA scans were performed at sites used clinically to determine osteoporotic status: lumbar spine, proximal femur (neck, trochanter, and total proximal femur), and distal radius (ultra-distal and distal one-third radius). Because of a mid-experiment change of screening facility location, two DXA scanners were used; 42 subjects were scanned with the QDR 4500 (Hologic) and 10 subjects were scanned using the Lunar Prodigy (GE Healthcare). Previous studies have found differences in absolute BMD measurements between devices from these manufacturers. However, no significant differences in T-scores were found at the lumbar spine.⁽¹⁷⁾ The standard NHANES III database was used to avoid discrepancies at the proximal femur.⁽¹⁸⁾

HR-pQCT imaging

HR-pQCT imaging was performed using the XtremeCT in vivo scanner (Scanco Medical AG). This device incorporates an X-ray source with cone beam geometry and a 2D detector array to create 3D reconstructions of mineralized tissue. In the in vivo configuration, the device images exclusively peripheral appendicular sites, specifically the distal tibia and ultradistal radius. The distal tibia and radius of each patient were imaged using the standard patient-style configuration, which yields isotropic (all edges of equal length) 82- μ m voxels. The following scan settings were used: source potential, 60 kVp; tube current, 900 μ A; integration time, 100 ms. A 9-mm scan (110 slices) was performed at each site. The scan began 9.5 mm proximal to the endplate in the radius and 22.5 mm proximal to the endplate in the tibia (Fig. 1). The nondominant limb was imaged except for subjects with a history of fracture in that limb. Images were immediately evaluated for motion arti-

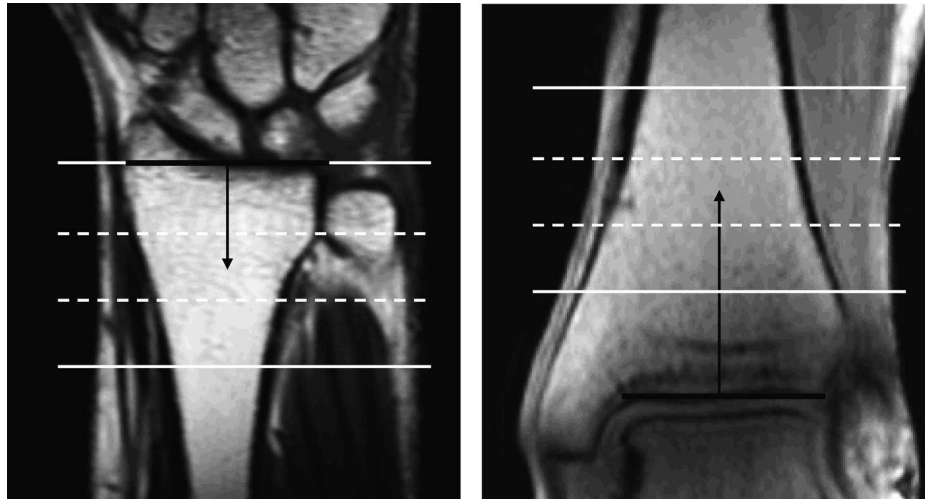


FIG. 1. MR scout views of the radius (left) and tibia (right). The MR high-resolution scan region (solid lines) and HR-pQCT scan region (dashed lines) are 27 and 9 mm in length, respectively. Scan regions are centered 14 mm proximal to the endplate in the radius and 27 mm proximal to the endplate in the tibia (black lines depict location of endplate reference and arrows depict distance to center of scan region).

facts; scans were repeated if obvious artifacts were detected. The effective dose was $<3 \mu\text{SV}$ per measurement.⁽¹⁹⁾ Imaging time was 3 min per scan. Including patient positioning, scan set-up, and occasional rescanning because of poor image quality, the imaging session was, on average, 30 min in total.

Attenuation values were converted to hydroxyapatite density ($\text{mg HA}/\text{cm}^3$) using a linear conversion based on a phantom provided by Scanco containing rods of HA-resin mixtures (0, 100, 200, 400, and $800 \text{ mg HA}/\text{cm}^3$) to determine density-based measures.

HR-pQCT analysis

HR-pQCT data were evaluated using the standard patient-style evaluation routines provided by the manufacturer. In this technique, the periosteal perimeter is identified using a semiautomated edge-finding algorithm that produces a closed contour around the periosteal surface. The cortical compartment is isolated by a two-step segmentation that applies a Gaussian blur, which removes trabecular features, followed by thresholding using a fixed pixel intensity criterion. Cortical thickness (Ct.Th) is calculated as cortical area (area of pixels included in the segmented cortical compartment) divided by periosteal perimeter (length of the closed contour around the periosteal surface). A binary representation of the trabecular region is created by applying a Laplace-Hamming filter and a fixed-value threshold to the data and applying a mask based on the cortical segmentation. The trabecular volume fraction (BV/TV) calculation is based on volumetric BMD in the trabecular compartment ($\text{vBMD}_{\text{trab}}$) and an assumed tissue density value of $1200 \text{ mg HA}/\text{cm}^3$. Trabecular number (Tb.N) is calculated using a midaxis transformation (MAT) to find trabecular ridges^(20,21) and the distance transform (DT) method to create a map of distances between ridges⁽²²⁾ and expressed as an average over all inter-ridge voxels (p).

$$\text{BV/TV} = \frac{\text{vBMD}_{\text{trab}}}{1200 \text{ mg HA/cc}} \quad (\text{Eq. 1})$$

$$\text{Tb.N} = \left[\frac{1}{p} \sum_{i=1}^{i=p} \text{DT}(\text{MAT}(\text{Image}))_i \right]^{-1} \quad (\text{Eq. 2})$$

Trabecular thickness (Tb.Th) and trabecular spacing (Tb.Sp) are derived from these primary measures using plate model assumptions.⁽²³⁾

$$\text{Tb.Th} = \frac{\text{BV/TV}}{\text{Tb.N}} \quad (\text{Eq. 3})$$

$$\text{Tb.Sp} = \frac{1 - \text{BV/TV}}{\text{Tb.N}} \quad (\text{Eq. 4})$$

Reproducibility of the HR-pQCT measures was determined in eight radii and seven tibias of volunteers spanning a large age range (radius: age = 25–65 yr; tibia: age = 29–73 yr). Three repeat measurements were performed with repositioning between each scan, and mean CV was calculated for each parameter at each anatomical site.

To identify potential differences in the cortical segmentation and the thickness calculations between MRI and HR-pQCT evaluations, the segmented cortices were isolated for visual inspection. The HR-pQCT cortical data were extracted from the XtremeCT patient evaluation database using in-house code programmed in IDL (Interactive Data Language; Research Systems).

In addition to the standard patient-style evaluation, which results in one mean value for the entire imaged volume, slice-by-slice data were extracted from the HR-pQCT database. BV/TV, Tb.N, and Ct.Th for each slice of the imaged region were used to study heterogeneity of structural parameters along the length of the imaged regions.

3T MR imaging

MR imaging was performed on a 3T Signa scanner (GE Medical). Images of the distal radius were obtained with the subject in a prone position using a transmit/receive quadrature wrist coil (Mayo Foundation for Medical Education and Research). Tibia imaging was performed with the subject in a supine position using a four-channel dual-paddle coil (Nova Medical). Custom-built immobilization devices

were used at both anatomical sites to reduce motion artifacts and to provide reproducible subject and coil positioning.

After a three-plane localizer obtained to visualize joint geometry for prescribing scan placement, 2-mm slice thickness steady-state free precession (SSFP; 1 NEX, 512×512 matrix) and 0.5-mm slice thickness balanced SSFP (bSSFP; 1 NEX, 512×384 matrix) images were obtained. The scan volumes were aligned visually with the radius or tibia axis, and a field of view (FOV) of 8 cm ($156 \times 156 \mu\text{m}^2$ pixel size) was used. The 2-mm (thick slice) sequence spanned the distal 7 cm of the radius or tibia and was used for cortical structure analysis. The nonbalanced SSFP sequence was chosen for cortical imaging primarily for the high bone/muscle contrast allowing easier segmentation of the periosteal boundary. The 2-mm pulse sequence parameters were as follows: repetition time/echo time (TR/TE) = 10.9–14.0/3.2–4.7 (radius) and 10.7–13.7/3.2–3.6 ms (tibia), bandwidth = 163 Hz/pixel, flip angle = 30, scan time = 4 (radius) and 4 min (tibia). The 0.5-mm (high resolution) sequence was obtained over a 2.5-cm length approximately centered on the HR-pQCT imaged volume and was used to determine trabecular structure. The volume was acquired with the same imaging plane orientation as the thick slice volume to allow a single axis registration (spatial alignment of volume images) between the two scans. The bSSFP sequence was chosen for its superior signal-to-noise ratio and image quality in the radius and tibia.^(24,25) The sequence was modified from the standard manufacturer sequence to allow imaging at the small (8 cm) FOV. Two phase-cycled acquisitions were acquired to reduce artifacts. The pulse sequence parameters were as follows: TR/TE = 14.4–15.2/3.3–3.9 (radius) and 16.8–17.8/6.5 ms (tibia), bandwidth = 122 Hz/pixel, flip angle = 60, scan time = 10 (radius) and 15 min (tibia). Including patient positioning and scan set-up, imaging time was ~50 min in total.

3T MRI analysis

The first step in the MRI structural analysis was the identification of slices corresponding to the 9-mm portion imaged through HR-pQCT. This was done in a semiautomated manner based on distance from the endplate. First, the high-resolution MRI scan (which does not contain the endplate) was axially aligned to the low-resolution thick slice image (which contains the endplate). This alignment was performed automatically by code developed in IDL. The code calculates the endosteal area for each slice of the high-resolution and thick slice MRI scans (using endosteal boundaries created by hand-drawn contours) and determines the discrepancy between the two area measurements as a function of axial offset. The offset producing the lowest discrepancy is interpreted as the optimal spatial registration of the two MRI data sets. Once the high-resolution MRI scan was registered to the thick slice image, the high-resolution slice located closest to 9.5 (radius) or 22.5 mm (tibia) from the endplate was identified as the first slice in the analysis region. A total of 18 adjacent slices defined the complete analysis region, covering the same 9 mm as the HR-pQCT scan.

This registration technique was confirmed in a subset of

cases by visual inspection of the trabecular and cortical structure in the matched MRI and HR-pQCT slices. As an additional validation of the MR/pQCT alignment, a second registration method was performed. In this technique, periosteal area was determined for each slice of the HR-pQCT data based on the automated periosteal segmentation and for one slice of the corresponding high-resolution MRI data based on a manually determined periosteal boundary. Code developed in IDL was used to determine the optimal axial alignment of the two data sets based on minimizing differences in periosteal area.

In some cases, the registration determined that the area captured in the high-resolution MRI scan did not include the entire HR-pQCT region. In this case, the subject was excluded from analyses that involved MRI-derived trabecular bone structural measures for the affected site (high-resolution MRI data excluded in $n = 2$ radii, $n = 6$ tibias).

Ct.Th was determined from the manually identified endosteal and periosteal surfaces in the thick slice data set using the DT technique. All trabecular parameters were calculated from the high-resolution data set. For the tibia analysis the images were first corrected for surface coil sensitivity inhomogeneities using a low-pass filter based algorithm,⁽²⁶⁾ modified for trabecular bone images.⁽²⁷⁾ Images were segmented using a global threshold criterion. BV/TV was calculated by pixel counting. Tb.N was determined using standard 2D histomorphometric methods, specifically the mean intercept length (MIL) technique based on the plate model.^(28,29) Tb.Th and Tb.Sp were derived from BV/TV and Tb.N as described for the HR-pQCT analysis (Eqs. 3 and 4). Reproducibility of these measures was determined in the radii and tibias of three volunteers (age = 27–53 yr). Two or three repeat measurements were performed with repositioning between each scan, and mean CV was calculated for each parameter at each anatomical site.

Statistical analysis

Relationships between structure measures (from both HR-pQCT and MRI) and subject age, weight, body mass index (BMI), and DXA measurements were studied using Pearson or Spearman correlations. Comparisons between HR-pQCT and MRI structural measures, as well as between MRI-derived structural measures based on the two registration techniques, were performed using Pearson correlations and paired Student's *t*-tests or Wilcoxon signed rank tests where appropriate. Heterogeneity of structural parameters along the length of the imaged regions was determined by calculating the absolute change in each parameter from the first to last slice. Heterogeneity was expressed as a percent of the mean value for the given parameter at the specific region across all subjects.

RESULTS

Patient statistics

The 52 women enrolled in this study had a mean age of 55 yr (range, 48–64 yr; Table 1). They were on average 31 mo past menopause (MPM: range, 0–60 mo), with menopause defined as 1 yr from the date of their last menstrual

TABLE 1. PATIENT STATISTICS FOR THE 52 WOMEN ENROLLED IN THE STUDY

	Age (yr)	MPM (month)	Weight (kg)	BMI	T-score spine	T-score femur			T-score radius	
						Neck	Trochanter	Total	Ultradistal	One third
Mean	55.0	31.0	65.7	24.3	-1.2	-1.4	-0.9	-0.8	-1.2	-0.6
±SD	3.6	17.4	9.7	2.4	0.7	0.6	0.6	0.6	0.9	0.9

T-score spine, total lumbar spine T-score; UD, ultradistal.

period. Mean lumbar spine T-score was -1.2 (range, -2.5 to 0.6), mean total femur T-score was -0.8 (range, -1.9 to 0.7), mean femoral neck T-score was -1.4 (range, -2.6 to 0.4), and mean ultradistal radius T-score was -1.2 (range, -3.2 to 0.9). Additional patient data are presented in Table 1.

Reproducibility of structural measures

The following are for the HR-pQCT parameters. In the radii, repeat measurements with repositioning yielded mean CV values of 1.2%, 5.8%, 5.3%, 5.8%, and 1.0% for BV/TV, Tb.N, Tb.Th, Tb.Sp, and Ct.Th, respectively. The tibia scans, which in general are subject to fewer motion artifacts, resulted in mean CV values of 0.3%, 1.4%, 1.5%, 1.5%, and 0.4% for BV/TV, Tb.N, Tb.Th, Tb.Sp, and Ct.Th, respectively. The following are for the MRI parameters. In the radii, repeat measurements with repositioning yielded mean CV values of 6.7%, 2.9%, 4.6%, and 6.1% for BV/TV, Tb.N, Tb.Th, and Tb.Sp, respectively. The tibia reproducibility scans resulted in mean CV values of 4.1%, 2.4%, 6.2%, 4.5%, and 4.3% for BV/TV, Tb.N, Tb.Th, Tb.Sp, and Ct.Th, respectively.

Registration of HR-pQCT and MRI scans

The discrepancy in alignment produced by the two registration methods was 0.9 ± 0.7 mm in the radius and 1.5 ± 2.3 mm in the tibia. This discrepancy resulted in different structural parameters only in the tibia and only for BV/TV, Tb.N, and Tb.Sp ($p < 0.05$). These parameters differed on average by 1% (BV/TV and Tb.N) or 2% (Tb.Sp). Accordingly, the influence of registration method on MR/pQCT correlations was deemed negligible. All results presented in the remainder of this work are based on the endplate alignment technique.

Comparison of HR-pQCT and MRI trabecular structure parameters

Statistically significant correlations between MRI and HR-pQCT values were found for all trabecular structure parameters studied (Fig. 2). Tb.N was the most highly correlated of the pooled radius and tibia data ($r^2 = 0.52$, $p < 0.0001$). Radius and tibia individual regression lines were indistinguishable for this parameter. The other parameters were weakly associated when radius and tibia data were pooled ($r^2 = 0.18$ – 0.34 , $p < 0.0001$) but stronger correlations were observed when sites were considered individually, the highest correlations being for Tb.Sp ($r^2 = 0.54$ radius, 0.60 tibia, $p < 0.0001$). MRI found large differences in BV/TV, Tb.Th, and Tb.Sp between the two sites (15–28%, $p < 0.0001$), whereas HR-pQCT found smaller differences in Tb.Th and Tb.Sp (7–13%, $p < 0.002$) and no sig-

nificant difference between sites for BV/TV. These discrepancies are responsible for the unique regressions for radius and tibia in the plots in Fig. 2.

Comparing the trabecular structure parameter values calculated by MRI to those calculated by HR-pQCT (Table 2), significant differences were found in every case ($p < 0.0001$). BV/TV was higher in the MRI analyses, with a mean MR/pQCT ratio of 3.2 in the radius and 3.9 in the tibia. Tb.N as calculated by MRI was slightly lower, with a mean MR/pQCT ratio of 0.9 in both the radius and tibia. Although differences in the Tb.N values calculated by the two modalities were statistically significant, the mean differences (13% radius, 8% tibia) were on the order of the CVs found in our reproducibility experiments. Tb.Th displayed the greatest absolute difference with a mean MR/pQCT ratio of 3.6 in the radius and 4.2 in the tibia. Tb.Sp was lower as calculated by MRI analysis with mean MR/pQCT ratio of 0.9 in the radius and 0.7 in the tibia.

Comparison of HR-pQCT and MRI cortical thickness values

A statistically significant correlation was found between MRI and HR-pQCT cortical thickness values in the tibia ($r^2 = 0.59$; Fig. 3). MRI analysis resulted in higher values of cortical thickness at this anatomical site (mean MR/pQCT ratio = 1.3). An important source of discrepancy between cortical thickness results was the large-scale intracortical porosity found in the majority of subjects in this study. This porosity is on a larger scale than the haversian canals and resorption cavities generally seen in histological studies. Porosity within the cortex resulted in loss of cortical area in the HR-pQCT segmentation, whereas in the MRI segmentation, the cortical porosity had little effect (Fig. 3).

In the MR images, Ct.Th could not be calculated for the entire ultradistal radius region. Close to the endplate the cortex becomes thin and flares from the narrow diaphysis to the wider epiphysis. This geometry limits visualization of the cortex in the axial MR images and therefore hampers accurate segmentation. Because MRI Ct.Th could be calculated only for the proximal one half of the HR-pQCT ultradistal radius region, the data are not presented.

Associations between structure parameters and age, weight, BMI, and DXA measurements

Correlations between cortical and trabecular structure parameters (as measured by both HR-pQCT and MRI) and age, weight, BMI, and T-score at the spine, femur, and ultradistal radius were calculated (Table 3). Relationships with areal BMD values were also studied; these yielded correlations very similar to those for T-score, with slightly

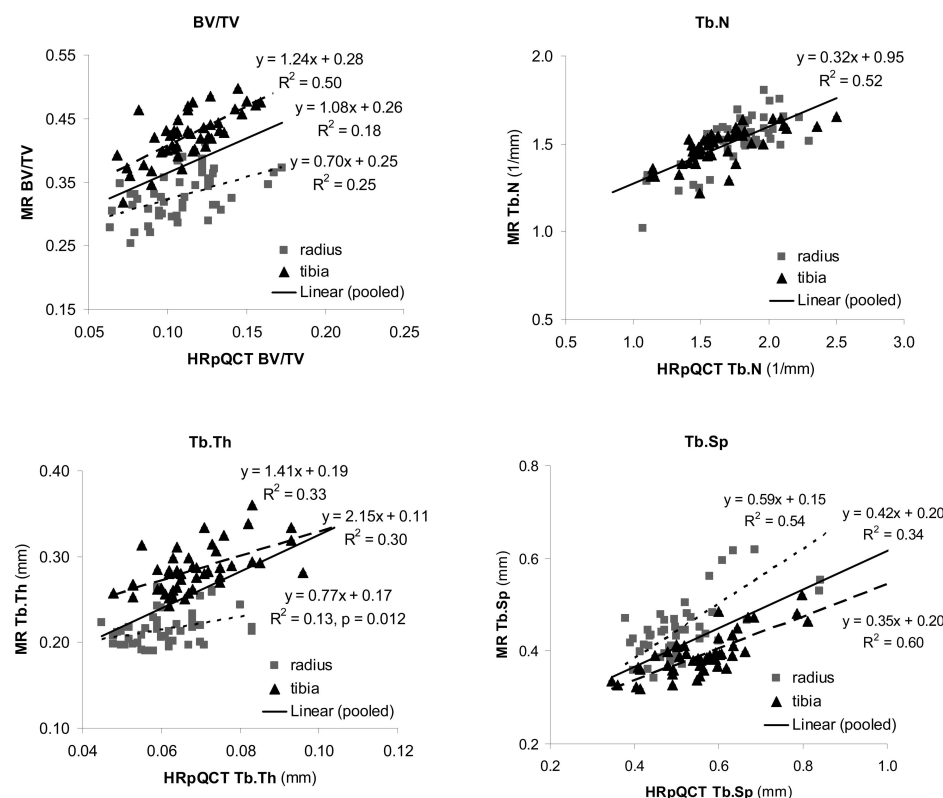


FIG. 2. Comparison of trabecular structure parameters calculated by MR and HR-pQCT in the radius (gray squares) and tibia (black triangles). All correlations are significant at $p < 0.0001$, except where noted. $n = 46$ radii and 46 tibias.

TABLE 2. COMPARISON OF STRUCTURE PARAMETERS DERIVED BY MR AND HR-pQCT FOR THE RADIUS AND TIBIA

		BV/TV	Tb.N (1/mm)	Tb.Th (mm)	Tb.Sp (mm)	Ct.Th (mm)
Radius	MR	0.33 ± 0.04	1.52 ± 0.15	0.22 ± 0.02	0.46 ± 0.09	—
	HR-pQCT	0.11 ± 0.03	1.77 ± 0.28	0.06 ± 0.01	0.52 ± 0.11	0.61 ± 0.14
Tibia	MR	0.42 ± 0.04	1.49 ± 0.10	0.29 ± 0.03	0.39 ± 0.05	1.32 ± 0.17
	HR-pQCT	0.11 ± 0.02	1.64 ± 0.29	0.07 ± 0.01	0.56 ± 0.10	1.01 ± 0.21

$n = 46$ radii and 46 tibias.

Data expressed in mean \pm SD.

Paired t -tests found significant differences between MR and HR-pQCT values for all parameters at $p < 0.0001$.

lower correlation coefficients (data not shown). The highest correlations were found between HR-pQCT-derived Ct.Th and BV/TV at the radius and ultradistal radius T-score ($r^2 = 0.45$ and 0.34 , respectively, $p < 0.0001$). All other correlations were weak, although many were statistically significant. None of the trabecular or cortical parameters calculated at the radius were correlated with age, weight, or BMI. Structure parameters in the tibia trended toward a greater occurrence of significant correlations with age, weight, BMI, and T-score than those in the radius. No correlations were found with femoral neck T-score or with MPM.

The minimal association between T-score and trabecular structure is clearly visualized when comparing images from two subjects with identical areal BMD and T-scores, yet substantially different bone structure (Fig. 4). In this comparison, SD of Tb.Sp (Tb.Sp SD)—a measure reflecting heterogeneity of the trabecular network—was more effective than any other structure or density parameter in distinguishing between the two subjects.

Correlations between HR-pQCT density parameters and patient statistics were also studied (Table 3). Among these comparisons, the highest correlation existed between total density in the radius and ultradistal radius T-score ($r^2 = 0.58$, $p < 0.0001$). This effect appeared to be shared equally between cortical and trabecular compartments, because each explained $\sim 50\%$ of the correlation.

Axial variation of structure parameters

Heterogeneity of structural parameters along the length of each imaged region was calculated from the HR-pQCT data (Fig. 5). The absolute change in each parameter from the first to last slice was calculated and expressed as a percent of the mean value for the given parameter at the specific region across all subjects. For the trabecular parameters, the minimum and mean values were nearly identical in the radius and tibia, whereas the maximum values were larger in the radius. Ct.Th variations were larger than those of trabecular parameters and larger in the radius than in the

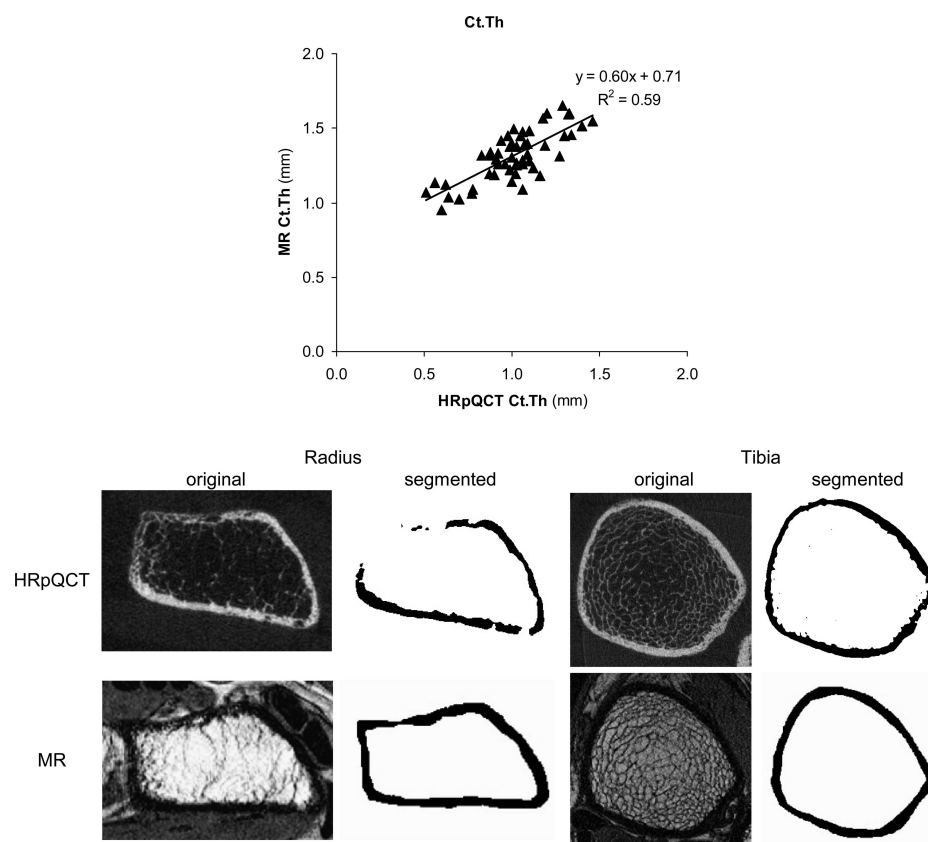


FIG. 3. (Top) Comparison of cortical thickness derived by MR and HR-pQCT for the tibia. Correlation is significant at $p < 0.0001$. $n = 52$ tibias. (Bottom) Spatially registered HR-pQCT and MR original and segmented images highlight differences between the two cortical segmentation strategies.

tibia. 3D representations of one radius and one tibia—both with average variation in structural parameters—are shown in Fig. 5.

DISCUSSION

In this study, we compared bone structure measures obtained in vivo by 3T MRI and HR-pQCT in a cohort of postmenopausal osteopenic women. Significant correlations between HR-pQCT and MRI parameters were found and were strongest for Tb.N, Ct.Th, and site-specific Tb.Sp, but weak for the other parameters studied. Comparisons between modalities additionally showed that MRI and HR-pQCT provide statistically different measurements of trabecular and cortical structure parameters. The largest discrepancies were found for BV/TV and Tb.Th, for which the MRI values were on average 3- to 4-fold higher than their HR-pQCT equivalents. Systematic differences between MRI and HR-pQCT segmentation procedures were observed, leading to discrepancies in cortical thickness values, with MRI values consistently higher than the HR-pQCT equivalent. Studying correlations between structure and density measures and the most clinically relevant DXA measures, we found strong relationships only between HR-pQCT measures in the radius and the ultradistal radius T-score. Finally, considerable variations in structural parameters along the length of the imaged regions were found (particularly in the radius), indicating that careful attention must be paid to registration of volumes of interest when

making cross-modality comparisons. Collectively, these findings suggest that differences in analysis techniques must be taken into account when comparing and interpreting the results of these imaging modalities.

MRI and HR-pQCT differ in many important ways in physics, acquisition, and analysis. MRI is a nonionizing modality that measures bone structure indirectly by detecting signal in marrow and soft tissue, whereas HR-pQCT images mineralized tissues directly by detecting X-ray attenuation. This difference in underlying physical principals is critical in understanding the effects of susceptibility, beam hardening, and other modality-specific artifacts. In terms of acquisition, most MRI sequences achieve high resolution in the image plane but relatively large slice thickness and therefore are analyzed using standard 2D morphometric techniques. HR-pQCT, in contrast, acquires isotropic voxels of smaller dimensions than those of MRI. Because HR-pQCT operates within the resolution-limited regimen however, direct 3D morphometric analysis of trabecular structure is not used in the standard evaluation. The analysis is done, instead, using a hybrid approach. Volume fraction is calculated based on the assumption of a fully mineralized tissue density of 1200 mg HA/cm^3 . Other morphometric parameters are derived from a combination of this density-based volume fraction and direct 3D measures, and for this reason, this technique is referred to as a “hybrid.” Clearly the substantial differences in acquisition and analysis may influence the quantitative data produced by these imaging techniques and therefore may also influence future clinical

TABLE 3. R^2 BETWEEN EACH PATIENT STATISTIC AND VOLUME FRACTION, TRABECULAR NUMBER, CORTICAL THICKNESS, AND VOLUMETRIC BONE DENSITY AT THE RADIUS OR TIBIA

						<i>T-score femur</i>		<i>T-score radius</i>	
						<i>Trochanter</i>	<i>Total</i>	<i>Ultradistal</i>	<i>One third</i>
		<i>Age</i>	<i>Weight</i>	<i>BMI</i>	<i>T-score spine</i>				
Radius									
MR	BV/TV	NS	NS	NS	NS	NS	NS	NS	NS
	Tb.N	NS	NS	NS	0.11*	NS	NS	NS	NS
HR-pQCT	Tb.Th	NS	NS	NS	NS	NS	NS	NS	0.11*-
	Tb.Sp	NS	NS	NS	0.09*-	NS	NS	0.12*-	NS
	BV/TV	NS	NS	NS	NS	NS	NS	0.34†	NS
	Tb.N	NS	NS	NS	0.12*	NS	NS	0.19†	NS
	Tb.Th	NS	NS	NS	NS	NS	NS	0.21†	NS
	Tb.Sp	NS	NS	NS	0.09*-	NS	NS	0.19†-	NS
	Ct.Th	NS	NS	NS	NS	NS	NS	0.45†	NS
	vBMD _{total}	NS	NS	NS	NS	0.10*	0.08*	0.58†	NS
	vBMD _{cort}	NS	NS	NS	NS	NS	NS	0.32†	NS
	vBMD _{trab}	NS	NS	NS	NS	NS	NS	0.34†	NS
Tibia									
MR	BV/TV	0.16†	0.19†	0.11*	NS	NS	NS	0.13*	NS
	Tb.N	NS	NS	NS	0.15†	NS	NS	NS	NS
	Tb.Th	NS	NS	NS	NS	NS	NS	0.11*	NS
	Tb.Sp	0.12*-	0.16†-	NS	NS	NS	NS	NS	NS
	Ct.Th	NS	NS	0.12*	NS	NS	NS	NS	NS
HR-pQCT	BV/TV	0.14†	NS	NS	0.14†	0.16†	0.08*	0.11*	NS
	Tb.N	NS	0.11*	NS	0.24†	0.11*	NS	0.11*	NS
	Tb.Th	0.08*	NS	NS	NS	NS	NS	NS	0.11*-
	Tb.Sp	NS	0.12*-	NS	0.17†-	0.12*-	NS	0.14†	NS
	Ct.Th	NS	NS	NS	NS	NS	0.10*	NS	NS
	vBMD _{total}	NS	NS	0.11*	0.10*	0.14†	0.15†	0.10*	NS
	vBMD _{cort}	0.17†-	NS	NS	NS	NS	NS	NS	NS
	vBMD _{trab}	0.14†	NS	NS	0.14†	0.16†	0.09*	0.10*	NS

$n = 46$ MR and 52 HR-pQCT.

* $p < 0.04$.

† $p < 0.008$.

No significant correlations were found with femoral neck T-score or months past menopause.

-, negative correlation.

or therapeutic decisions based on their results. In ex vivo studies comparing these modalities to μ CT imaging, the gold standard in high-resolution 3D structural imaging (Table 4), we see that HR-pQCT parameters are in general more accurate than those measured using MRI. However, correlation coefficients are similar and possibly better for some MRI parameters, reinforcing the use of this imaging modality.

Of the trabecular structure parameters studied, Tb.N and site-specific Tb.Sp displayed the highest correlation and lowest error between MRI and HR-pQCT values. In fact, the differences between the MRI and HR-pQCT Tb.N values were on the order of the variation in our reproducibility studies. Our finding that Tb.N and Tb.Sp are the most highly correlated of the trabecular structure parameters is consistent with ex vivo studies showing that Tb.N and Tb.Sp are the measures most accurately assessed by both MRI⁽¹⁵⁾ and HR-pQCT⁽¹⁴⁾ as determined by comparison with μ CT imaging (Table 4). In both HR-pQCT and MRI analyses, the calculation of Tb.N uses a threshold chosen to preserve structure and connectivity, which therefore preserves most trabeculae to maximize the accuracy of the Tb.N calculation. In MRI, trabeculae are further enhanced through susceptibility artifacts, accentuated at high field

strengths (3T) and using gradient echo sequences.⁽²⁵⁾ Tb.Sp values are accurate for the same reasons, as they are driven by Tb.N rather than Tb.Th. This can be seen by expressing Tb.Sp as $Tb.N^{-1} - Tb.Th$ (see Eqs. 3 and 4) and noting that the absolute values and variation of $Tb.N^{-1}$ are greater than those of Tb.Th in this population.

The highest discrepancies between MRI and HR-pQCT existed in BV/TV and Tb.Th. Again this is consistent with ex vivo studies (Table 4) showing that MRI overestimates these parameters, whereas HR-pQCT underestimates both BV/TV and Tb.Th.⁽¹⁴⁾ As would therefore be expected, our study shows that the discrepancy between MRI and HR-pQCT is greater than that shown to exist between MRI and μ CT. It is clear that Tb.Th is the least robust of the trabecular architectural parameters calculated by MRI and HR-pQCT. In HR-pQCT, the derivation of Tb.Th from vBMD_{trab} results in values lower than the resolution of the system, and in fact, lower than true trabecular dimensions. In MRI, limited resolution leads to partial voluming and exclusion of the smallest trabeculae, whereas susceptibility artifacts enhance the remaining trabeculae, in combination leading to overestimation of Tb.Th.

It is interesting to note that greater discrepancies ($p < 0.0001$) between MRI and HR-pQCT values for all trabec-

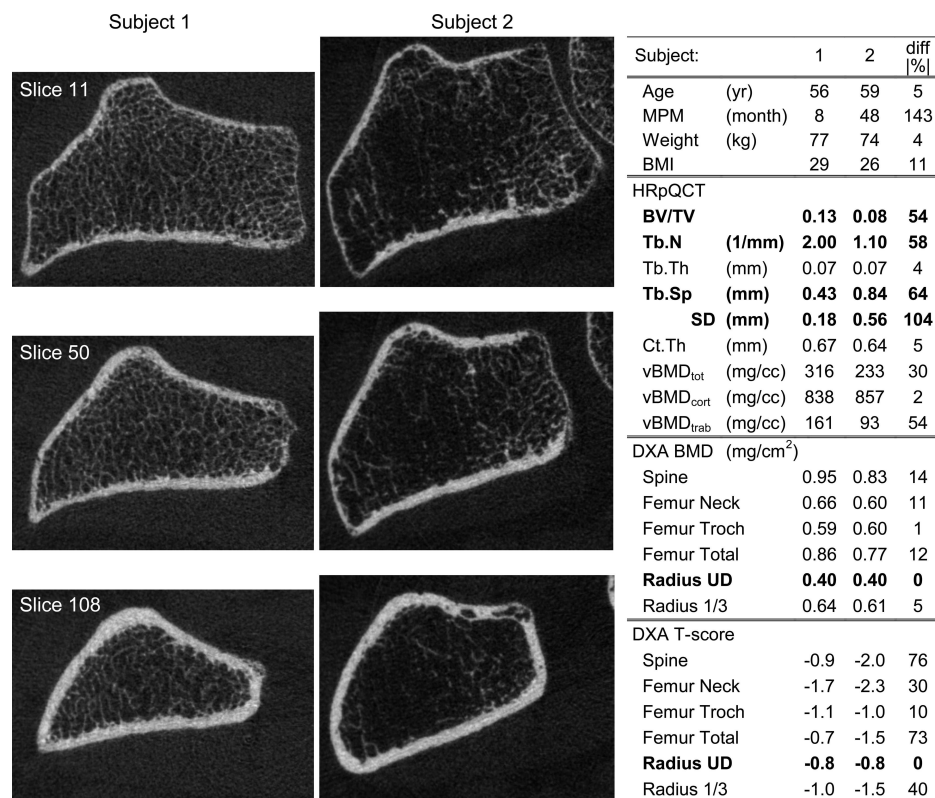


FIG. 4. HR-pQCT images of the radii of two subjects with identical ultradistal radius areal BMD values and T-scores (UD radius BMD = 0.40; T-score = -0.8). Slice 11 (top row) is most distal, and slice 108 (bottom row) is most proximal. Trabecular structure appears well maintained and interconnected in subject 1, whereas trabeculae are scarce and not well interconnected in subject 2. Subject data and results of HR-pQCT, MRI, and DXA analyses for these subjects are tabulated above. HR-pQCT data show that the trabecular parameters BV/TV, Tb.N, Tb.Th, and Tb.Sp SD (a measure of structural heterogeneity) differ by ~50–100% between these subjects. These images and data clearly show that trabecular and cortical structure may differ in patients with identical areal BMD values.

Radius	Variation over imaged length (% mean value in radius)		
	max	min	mean
BV/TV	58	8	23
Tb.N	59	15	26
Ct.Th	152	77	112

Tibia	Variation over imaged length (% mean value in tibia)		
	max	min	mean
BV/TV	40	8	24
Tb.N	33	12	22
Ct.Th	71	30	47

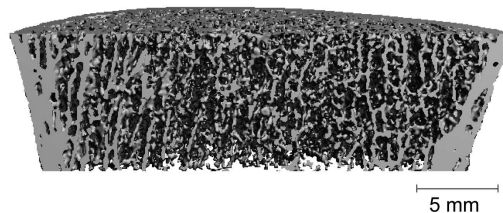
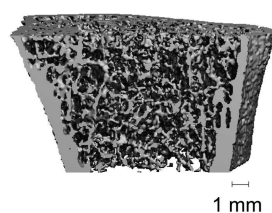


FIG. 5. Heterogeneity of structural parameters along the length of the imaged region in the radius (left) and tibia (right). For each subject, parameter variation over the imaged length was calculated from HR-pQCT slice-by-slice results. Each result was divided by the mean parameter value for all radii or tibias to express the variation in percent of mean parameter value. Renderings of 3D reconstructions of HR-pQCT data are shown to illustrate radius and tibia structure in subjects with average variation in structural parameters.

ular structure parameters excluding Tb.N were found in the tibia. This is visualized in the site-specific regression lines in Fig. 2. One explanation for this phenomenon may be related to the greater cortical thickness in the tibia, which may produce a greater degree of beam hardening artifact in the HR-pQCT images. The effect of this beam hardening artifact would be to decrease the observed BV/TV and subsequently decrease Tb.Th and increase Tb.Sp, and in this way, exaggerate the discrepancies between MRI and HR-pQCT values. This possibility must be further studied and may be complicated by the beam hardening correction algorithm implemented in the data reconstruction. Additional confounders in comparing radius to tibia measures include differences in soft tissue volume, marrow composition, and

motion artifacts. These have the potential to influence the observed vBMD_{trab} and therefore affect BV/TV, Tb.Th, and Tb.Sp in the HR-pQCT analysis. In the MRI analysis, the longer TE and the low pass coil sensitivity correction applied to the tibia scans may result in greater overestimation of Tb.Th and BV/TV at this site.

Cortical thickness values were higher as calculated by MRI and lower by HR-pQCT, resulting in part from the inherently different segmentation and calculation processes. The Gaussian blur used in the HR-pQCT Ct.Th analysis tends to remove portions of the cortex that are extremely thin or contain large porosities. Cortical porosity was a common finding in the postmenopausal subjects investigated in this study, as depicted in Figs. 3 and 4. An

TABLE 4. SUMMARY OF MR TO HR-pQCT RATIOS AND COEFFICIENTS FROM THIS STUDY AND DATA ADAPTED FROM STUDIES COMPARING EACH TECHNIQUE TO μ CT IMAGING

	<i>MR vs. HR-pQCT</i> (this study: radius)		<i>MR vs. HR-pQCT</i> (this study: tibia)		<i>MR vs. μCT</i> (Phan et al.: calcaneus)		<i>HR-pQCT vs. μCT</i> (MacNeil and Boyd: radius)	
	<i>MR/pQCT ratio</i>	<i>r²</i>	<i>MR/pQCT ratio</i>	<i>r²</i>	<i>MR/μCT ratio</i>	<i>r²</i>	<i>pQCT/μCT ratio</i>	<i>r²</i>
BV/TV	3.16 \pm 0.66*	0.25	3.87 \pm 0.62*	0.50	3.08 \pm 0.91	0.87	0.59	0.86
Tb.N	0.87 \pm 0.10 [†]	0.57	0.92 \pm 0.12 [†]	0.51	1.55 \pm 0.30	0.79	1.11	0.95
Tb.Th	3.59 \pm 0.50*	0.13	4.22 \pm 0.53*	0.33	1.95 \pm 0.24	0.76	0.40	0.59
Tb.Sp	0.89 \pm 0.12*	0.54	0.72 \pm 0.09*	0.60	0.46 \pm 0.08	0.87	1.09	0.84
Ct.Th	—	—	1.34 \pm 0.22	0.59	—	—	0.86	0.96

Data expressed in mean \pm SD. SD values not available in MacNeil and Boyd.

Significant differences between radius and tibia MR/pQCT ratios were found for all trabecular parameters in this study: * $p < 0.0001$; [†] $p = 0.002$.

alternative segmentation technique may be appropriate for this application. In the MRI images, cortical porosity is not as clearly depicted and is therefore often included into the cortical area. MRI cortical segmentation presents its own challenges, because the periosteal surface is often obscured by neighboring regions of connective tissue, which, like bone, produce a low-intensity signal. An alternative cortical segmentation method may also be appropriate for MRI analysis,⁽³⁰⁾ but alternatives would also be hindered by low signal adjacent to the periosteum. Furthermore, the two strategies for calculation of Ct.Th from the segmented data are different and may contribute to the discrepancy in MRI and HR-pQCT values. The HR-pQCT strategy will lead to underestimation of Ct.Th, because areas of the cortex excluded from the segmentation caused by porosity will bias the mean Ct.Th value downward.

The ultradistal region of the radius—the region scanned in standard XtremeCT patient evaluation—is an area in which accurate MR cortical segmentation is difficult. Low cortical thickness and flared epiphyseal geometry, compounded by chemical shift artifacts, hamper MR-based cortical visualization in this region. This must be considered in future studies incorporating measures from MRI and HR-pQCT systems.

In the comparison of structure and density parameters to DXA measures, trabecular bone structure was shown to have little correlation with T-score. This is evident in the comparison of two subjects with identical radius areal BMD and T-scores shown in Fig. 4 and is well-documented in literature discussing the limitations of projectional BMD measurements.^(11,31–33) Of the structure parameters calculated at the distal radius, Ct.Th was found to be the most influential on radius T-score. Trabecular structure parameters derived from HR-pQCT were more strongly correlated with T-score at the ultradistal radius than those derived from MRI. This is likely influenced by the fact that both DXA and HR-pQCT are radiographic modalities dependent on tissue density, whereas the physics of MRI are based on entirely different principles. One previous in vivo study resulted in stronger correlations between MRI structure parameters and DXA measures, on the order of $r^2 = 0.40$ but was based on more inclusive subject criteria and included both pre- and postmenopausal subjects.⁽³⁴⁾ The smaller range of structure and density parameters in the postmenopausal osteopenic population studied here will of

course produce lower correlations. The HR-pQCT density parameter vBMD_{total}, the volumetric equivalent to DXA-based areal BMD, was found to have the strongest relationship with T-score ($r^2 = 0.58$), in accordance with previously published data.⁽¹¹⁾ The 3D nature of the HR-pQCT data has the important advantage of allowing us to deconstruct Dtotal into the cortical and trabecular components, and by doing this, we found that, in the distal radius, cortical and trabecular compartments contribute equally to the DXA BMD measurement. Our data showed no or very weak correlations between HR-pQCT vBMD measurements and DXA at sites other than the distal radius. Based on this finding, it is clear that BMD measurements are not surrogates for density measurements at remote sites. This underscores the clinical practice of imaging directly at the site of interest when possible.

Variation in structural parameters along the length covered by HR-pQCT imaging was on the order of 25% for trabecular parameters. Thickness of the cortex displayed more heterogeneity than the trabecular parameters and was more extreme in the radius where variations were on average 112% and up to 152% of the mean Ct.Th value for all radii. This indicates that the radius scan covers a transitional region where trabecular bone begins to dominate and Ct.Th decreases close to the endplate. The heterogeneity in trabecular parameters is significant compared with the variations expected over time in osteoporosis progression or therapy studies.^(35,36) Therefore, spatial registration of analysis volumes—within one imaging modality and between modalities—is crucial for assessing structural parameters in these anatomical regions.

A limitation of this study is the lack of a standard of reference for comparison of these in vivo data. The current gold standard for 3D bone morphology measures, μ CT analysis, can be performed only on ex vivo specimens (e.g., iliac crest biopsies) because of size constraints and therefore is not an appropriate tool for assessing the accuracy of in vivo measurements. It is possible to use cadaver specimens to mimic in vivo imaging in the MRI and HR-pQCT systems and excise the region of interest to conduct μ CT imaging for comparison. These experiments are currently being conducted in our laboratory and by other investigators.^(14,25) Cadaver studies, however, cannot duplicate in vivo imaging for a number of reasons (air bubbles in the marrow influence analysis results, motion typical of patient

studies is absent); therefore, we believe this in vivo study is most representative of the capabilities of MRI and HR-pQCT. A second potential limitation is the restricted population included in this study, which limits the generalization of these results to a wider population. However, we believe this early postmenopausal cohort is representative of many potential study populations, particularly clinical trials of osteoporosis-related therapies.

In summary, this study provides insight into two emerging noninvasive tools for the evaluation of bone structure. Significant correlations between HR-pQCT and MRI parameters were found and were strongest for Tb.N, Ct.Th, and site-specific Tb.Sp. Our analysis showed, however, that MRI and HR-pQCT provide statistically different measurements of trabecular and cortical structure parameters. The largest discrepancies were found for BV/TV and Tb.Th, for which MRI analysis provided values three to four times higher than HR-pQCT analysis. Our findings highlight the significant influence of analysis technique on the results of in vivo assessment and underscore the importance of accounting for these differences when comparing and interpreting results from these two modalities.

ACKNOWLEDGMENTS

The authors thank Thelma Munoz, Jingyi Yu, Nicole Cheng, Melissa Guan, and Ayako Suzuki for contributions in recruiting subjects, DXA and HR-pQCT imaging, and database management. We also thank Andres Laib and Scanco Medical AG for providing consultation and software development support. This work is funded by a grant from Merck & Co.

REFERENCES

- 1991 Consensus development conference: Prophylaxis and treatment of osteoporosis. *Am J Med* **90**:107–110.
- Cummings S, Black D, Nevitt M, Browner W 1993 Bone density at various sites for prediction of hip fractures. *Lancet* **341**:72–75.
- Schott AM, Cormier C, Hans D, Favier F, Hausherr E, Dargent-Molina P, Delmas PD, Ribot C, Sebert JL, Breart G, Meunier PJ 1998 How hip and whole-body bone mineral density predict hip fracture in elderly women: The EPIDOS Prospective Study. *Osteoporos Int* **8**:247–254.
- Beck TJ, Looker AC, Ruff CB, Sievanen H, Wahner HW 2000 Structural trends in the aging femoral neck and proximal shaft: Analysis of the Third National Health and Nutrition Examination Survey dual-energy X-ray absorptiometry data. *J Bone Miner Res* **15**:2297–2304.
- Stone KL, Seeley DG, Lui LY, Cauley JA, Ensrud K, Browner WS, Nevitt MC, Cummings SR 2003 BMD at multiple sites and risk of fracture of multiple types: Long-term results from the Study of Osteoporotic Fractures. *J Bone Miner Res* **18**:1947–1954.
- Black DM, Cummings SR, Karpf DB, Cauley JA, Thompson DE, Nevitt MC, Bauer DC, Genant HK, Haskell WL, Marcus R, Ott SM, Torner JC, Quandt SA, Reiss TF, Ensrud KE 1996 Randomised trial of effect of alendronate on risk of fracture in women with existing vertebral fractures. Fracture Intervention Trial Research Group. *Lancet* **348**:1535–1541.
- Delmas PD, Seeman E 2004 Changes in bone mineral density explain little of the reduction in vertebral or nonvertebral fracture risk with anti-resorptive therapy. *Bone* **34**:599–604.
- Gordon CL, Lang TF, Augat P, Genant HK 1998 Image-based assessment of spinal trabecular bone structure from high-resolution CT images. *Osteoporos Int* **8**:317–325.
- Link TM, Vieth V, Langenberg R, Meier N, Lotter A, Newitt D, Majumdar S 2003 Structure analysis of high resolution magnetic resonance imaging of the proximal femur: In vitro correlation with biomechanical strength and BMD. *Calcif Tissue Int* **72**:156–165.
- Muller ME, Webber CE, Bouxsein ML 2003 Predicting the failure load of the distal radius. *Osteoporos Int* **14**:345–352.
- Sornay-Rendu E, Boutroy S, Munoz F, Delmas PD 2007 Alterations of cortical and trabecular architecture are associated with fractures in postmenopausal women, partially independent of decreased BMD measured by DXA: The OFELY study. *J Bone Miner Res* **22**:425–433.
- Chesnut CH III, Rosen CJ 2001 Reconsidering the effects of antiresorptive therapies in reducing osteoporotic fracture. *J Bone Miner Res* **16**:2163–2172.
- Riggs BL, Melton LJ III 2002 Bone turnover matters: The raloxifene treatment paradox of dramatic decreases in vertebral fractures without commensurate increases in bone density. *J Bone Miner Res* **17**:11–14.
- MacNeil JA, Boyd SK 2007 Accuracy of high-resolution peripheral quantitative computed tomography for measurement of bone quality. *Med Eng Phys* **29**:1096–1105.
- Phan CM, Matsuura M, Bauer JS, Dunn TC, Newitt D, Lochmueller EM, Eckstein F, Majumdar S, Link TM 2006 Trabecular bone structure of the calcaneus: Comparison of MR imaging at 3.0 and 1.5 T with micro-CT as the standard of reference. *Radiology* **239**:488–496.
- World Health Organization 1994 Assessment of fracture risk and its application to screening for postmenopausal osteoporosis. Report of a WHO Study Group. *World Health Organ Tech Rep Ser* **843**:1–129.
- Faulkner KG, Roberts LA, McClung MR 1996 Discrepancies in normative data between Lunar and Hologic DXA systems. *Osteoporos Int* **6**:432–436.
- Binkley N, Kiebzak GM, Lewiecki EM, Krueger D, Gangnon RE, Miller PD, Shepherd JA, Drezner MK 2005 Recalculation of the NHANES database SD improves T-score agreement and reduces osteoporosis prevalence. *J Bone Miner Res* **20**:195–201.
- Laib A, Hammerle S, Koller B 2004 A new 100 μ m resolution scanner for in vivo 3D-CT of the human forearm and lower leg. 16th International Bone Densitometry Workshop, Annecy, France, June 20–24, 2004.
- Laib A, Hildebrand T, Hauselmann HJ, Rueggsegger P 1997 Ridge number density: A new parameter for in vivo bone structure analysis. *Bone* **21**:541–546.
- Muller R, Hildebrand T, Rueggsegger P 1994 Non-invasive bone biopsy: A new method to analyse and display the three-dimensional structure of trabecular bone. *Phys Med Biol* **39**:145–164.
- Hildebrand T, Rueggsegger P 1997 A new method for the model-independent assessment of thickness in three-dimensional images. *J Microsc* **185**:67–75.
- Laib A, Rueggsegger P 1999 Calibration of trabecular bone structure measurements of in vivo three-dimensional peripheral quantitative computed tomography with 28-microm-resolution microcomputed tomography. *Bone* **24**:35–39.
- Banerjee S, Han ET, Krug R, Newitt DC, Majumdar S 2005 Application of refocused steady-state free-precession methods at 1.5 and 3 T to in vivo high-resolution MRI of trabecular bone: Simulations and experiments. *J Magn Reson Imaging* **21**:818–825.
- Krug R, Han ET, Banerjee S, Majumdar S 2006 Fully balanced steady-state 3D-spin-echo (bSSSE) imaging at 3 Tesla. *Magn Reson Med* **56**:1033–1040.
- Wald LL, Carvajal L, Moyher SE, Nelson SJ, Grant PE, Barkovich AJ, Vigneron DB 1995 Phased array detectors and an automated intensity-correction algorithm for high-resolution MR imaging of the human brain. *Magn Reson Med* **34**:433–439.
- Newitt DC, van Rietbergen B, Majumdar S 2002 Processing

- and analysis of in vivo high-resolution MR images of trabecular bone for longitudinal studies: Reproducibility of structural measures and micro-finite element analysis derived mechanical properties. *Osteoporos Int* **13**:278–287.
28. Parfitt AM 1988 Bone histomorphometry: Proposed system for standardization of nomenclature, symbols, and units. *Calcif Tissue Int* **42**:284–286.
 29. Newitt DC, Majumdar S, van Rietbergen B, von Ingersleben G, Harris ST, Genant HK, Chesnut C, Garnero P, MacDonald B 2002 In vivo assessment of architecture and micro-finite element analysis derived indices of mechanical properties of trabecular bone in the radius. *Osteoporos Int* **13**:6–17.
 30. Gomberg BR, Saha PK, Wehrli FW 2005 Method for cortical bone structural analysis from magnetic resonance images. *Acad Radiol* **12**:1320–1332.
 31. Kleerekoper M, Villanueva AR, Stanciu J, Rao DS, Parfitt AM 1985 The role of three-dimensional trabecular microstructure in the pathogenesis of vertebral compression fractures. *Calcif Tissue Int* **37**:594–597.
 32. Seeman E, Delmas PD 2006 Bone quality—the material and structural basis of bone strength and fragility. *N Engl J Med* **354**:2250–2261.
 33. Ulrich D, van Rietbergen B, Laib A, Rueggsegger P 1999 The ability of three-dimensional structural indices to reflect mechanical aspects of trabecular bone. *Bone* **25**:55–60.
 34. Ouyang X, Selby K, Lang P, Engelke K, Klifa C, Fan B, Zucconi F, Hottya G, Chen M, Majumdar S, Genant HK 1997 High resolution magnetic resonance imaging of the calcaneus: Age-related changes in trabecular structure and comparison with dual X-ray absorptiometry measurements. *Calcif Tissue Int* **60**:139–147.
 35. Borah B, Dufresne TE, Chmielewski PA, Johnson TD, Chines A, Manhart MD 2004 Risedronate preserves bone architecture in postmenopausal women with osteoporosis as measured by three-dimensional microcomputed tomography. *Bone* **34**:736–746.
 36. Chesnut CH III, Majumdar S, Newitt DC, Shields A, Van Pelt J, Laschansky E, Azria M, Kriegman A, Olson M, Eriksen EF, Mindeholm L 2005 Effects of salmon calcitonin on trabecular microarchitecture as determined by magnetic resonance imaging: Results from the QUEST study. *J Bone Miner Res* **20**:1548–1561.

Address reprint requests to:

Galateia J Kazakia, PhD

*Musculoskeletal and Quantitative Imaging Research
Group*

Department of Radiology

University of California, San Francisco

Byers Hall, Suite 203, 1700 4th Street

San Francisco, CA 94158, USA

E-mail: galateia.kazakia@radiology.ucsf.edu

Received in original form June 4, 2007; revised form October 5, 2007; accepted November 21, 2007.